NANO LETTERS

pubs.acs.org/NanoLett

DNA Translocation through Graphene Nanopores

Christopher A. Merchant, Ken Healy, Meni Wanunu, Vishva Ray, Neil Peterman, John Bartel, Michael D. Fischbein, Kimberly Venta, Zhengtang Luo, A. T. Charlie Johnson, and Marija Drndić*

Department of Physics and Astronomy, University of Pennsylvania, Philadelphia, Pennsylvania, 19104

ABSTRACT We report on DNA translocations through nanopores created in graphene membranes. Devices consist of 1−5 nm thick graphene membranes with electron-beam sculpted nanopores from 5 to 10 nm in diameter. Due to the thin nature of the graphene membranes, we observe larger blocked currents than for traditional solid-state nanopores. However, ionic current noise levels are several orders of magnitude larger than those for silicon nitride nanopores. These fluctuations are reduced with the atomic-layer deposition of 5 nm of titanium dioxide over the device. Unlike traditional solid-state nanopore materials that are insulating, graphene is an excellent electrical conductor. Use of graphene as a membrane material opens the door to a new class of nanopore devices in which electronic sensing and control are performed directly at the pore.

KEYWORDS DNA sequencing, atomic layer deposition, single molecule, nanopores

Solid state[1−8] and biological[9] nanopores are proving to be invaluable tools for probing single molecules. A nanopore is a small hole that connects two chambers that contain electrolyte solution. An applied voltage across the nanopore drives ions through the pore, which is recorded from the voltage source using a high-gain amplifier. DNA molecules, added to the electrolyte solution, can then be driven single file through such nanopores by the electric field.[9] As the molecules translocate they partially block ion flow through the pore, detected as a drop in the measured current. Electronically monitoring the process of DNA translocation has been proposed as a low-cost, high-throughput DNA sequencing technique.[9] Recently, the four DNA bases were shown to impede the ion current differently in a biological pore,[10,11] and other theoretical and experimental works suggest that the four bases can be discriminated by measuring their transverse conductance.[12−14] In light of these works, synthetic nanopore materials with atomic thickness and electrical addressability may serve as a step toward nanopore-based DNA sequencing.

Common membrane materials currently used for nanopore device fabrication are insulators such as silicon nitride[15] (SiN), aluminum oxide,[16] and silicon oxide[17] (SiO_2). Graphene is a thin, flexible material with good electronic conductivity and robust mechanical properties.[18−21] Fischbein et al.[22] have shown that nanopores, nanopore arrays, and other structures, can be fabricated in suspended graphene sheets by controlled electron-beam exposure in a transmission electron microscope (TEM). Despite the extreme thinness of the suspended graphene sheets, nanopores were structurally robust and their shape was stable over time. Use of graphene as a nanopore membrane material could permit sensing and control of the electric potential directly at the nanopore. Additionally, atomically thin graphene nanoelectrodes have been considered for DNA sequencing based on DNA's transverse conductance[13] and multilayer graphene−insulator devices could control the molecule's motion sufficiently to reliably measure the conductance of each consecutive nucleotide.[23,24] Despite these possibilities, the interactions between graphene nanopores and biomolecules in aqueous solution have yet to be explored.

In this Letter, we show the first experimental realization of DNA translocation through graphene nanopores, which is the first step toward exploring the potential applications of this new membrane material. We show that the ionic blocked current signatures from DNA translocations through sub-10-nm diameter graphene nanopores compare favorably with similar diameter SiN nanopores. However, we also observe that the current signal from bare graphene nanopores is consistently noisier than that for SiN nanopores, and the DNA translocation signals reveal nonuniform current amplitudes. The large noise is attributed to the presence of pinholes in the graphene membranes as well as incomplete wetting. We find that atomic layer deposition (ALD) of several nanometers of titanium dioxide over the devices consistently reduces the nanopore noise level and improves the mechanical robustness of the device. This process preserves electrical addressability of the nanopore, which may be useful for realizing both multilayer graphene−insulator nanopores[23,24] and graphene nanogap devices.[13]

A schematic of a typical graphene nanopore device is given in Figure 1a. Silicon chips covered with 5 μm of SiO_2 and 40 nm of silicon nitride are etched so that freestanding

* To whom correspondence should be addressed: e-mail, drndic@physics.upenn.edu; phone, 215-898-5810; fax, 215-898-2010.

Received for review: 3/25/2010
Published on Web: 07/23/2010

DOI: 10.1021/nl101046t | *Nano Lett.* **2010,** *10,* 2915–2921

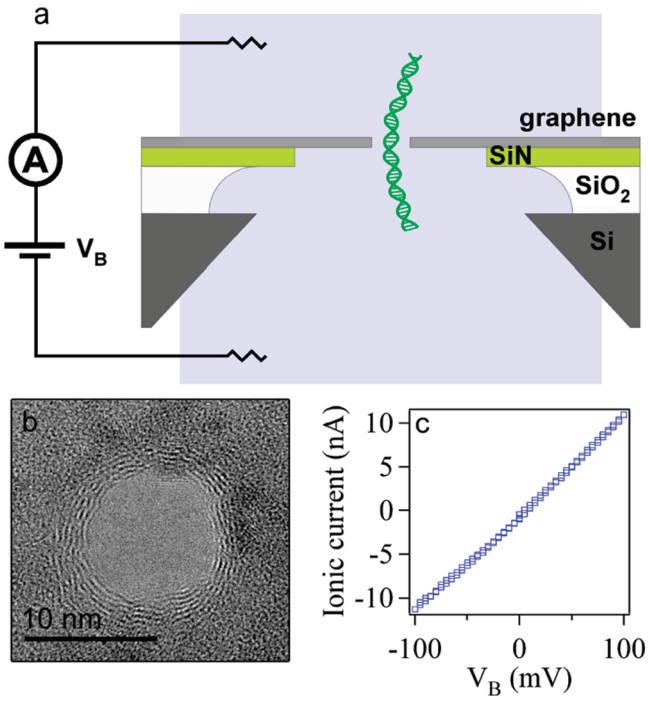

FIGURE 1. Graphene nanopore devices. (a) Device schematic. Few-layer graphene (1−5 nm thick) is suspended over a 1 μm diameter hole in a 40 nm thick silicon nitride (SiN) membrane. The SiN membrane is suspended over an approximately 50 × 50 μm^2 aperture in a silicon chip coated with a 5 μm SiO_2 layer. The device is inserted into a PDMS measurement cell with microfluidic channels that form reservoirs in contact with either side of the chip. A bias voltage, V_B, is applied between the reservoirs to drive DNA through the nanopore. (b) TEM image of a nanopore in a graphene membrane. Scale bar is 10 nm. (c) Ionic current−voltage measurement for this 10 nm graphene nanopore device in 1 M KCl, pH 9.

nitride membranes of approximately 50 μm square remain. Electron beam lithography (EBL) followed by an SF_6 plasma etch is used to pattern a ∼1.5 μm diameter hole through the nitride membrane. Graphene is grown by the chemical vapor deposition (CVD) of methane over polished copper foils,[25] as detailed in Figure S1 in the Supporting Information. The copper foils are etched in solution so that bare graphene sheets, approximately 1−5 nm thick (3−15 monolayers), shown in Figure S2 (Supporting Information), float on the surface of the liquid. Suitably sized graphene sheets, larger than 2 mm × 2 mm, are then scooped onto the prepatterned silicon nitride membranes, as shown in Figure S3 (Supporting Information). In this way the graphene is structurally supported by the nitride membrane, with only a limited area freely suspended over the 1.5 μm hole. Nanopores are then drilled through the suspended graphene membranes by transmission electron beam ablation lithography[22,26] (TEBAL). We have used CVD graphene, rather than exfoliated, because the centimeter-scale sheets are easy to manipulate and the process is scalable for future applications. It has been observed that CVD graphene is very hydrophobic,[27] and we have found that a rapid UV/ozone treatment facilitates complete wetting of the graphene nanopores. All devices underwent at least 5 min of UV/ozone treatment immediately prior to assembly in a PDMS measurement cell and exposure to electrolyte. Our measurement cell has microfluidic channels that form reservoirs in contact with either side of the chip. With a pair of Ag/AgCl electrodes, a bias voltage, V_B, is applied between the two reservoirs to drive ionic current through the nanopore.

A TEM image of a representative nanopore drilled into a suspended graphene membrane is given in Figure 1b. The visible rings around the pore are from graphene layers, and their number provides an estimate of the graphene membrane thickness.[21,22,28] Figure 1c shows a typical measurement of the ionic current through a graphene nanopore as a function of the applied voltage, V_B. We find that graphene nanopores with diameters ranging from 5 to 10 nm exhibit a wide range of conductance values between ∼20 and 1000 nS (see Figure S4 in the Supporting Information). This wide conductance range does not correlate with nanopore size and cannot be explained by membrane thickness variations, which suggests that ions are able to flow through pinholes in the graphene membranes. UV/ozone treatment of graphitic material, such as carbon nanotubes (CNTs), has been shown to induce defects by an oxidative reaction.[29] Electron beam irradiation has also been shown to affect the properties of carbon-based materials and induce defects.[30] It is reasonable, therefore, that UV/ozone treatment and/or electron beam irradiation forms occasional pinholes in some of our ultrathin membranes,[31] though they are not readily visible under TEM observation. Our own measurements, highlighted in Figure S5 (Supporting Information), indicate that UV/ozone treatments create defects in graphene, which increase the electrical resistance of these sheets over time. While these pinholes increase the baseline ion current signal and associated noise, they do not otherwise hinder the ability of our devices to measure DNA translocation through the fabricated nanopores. The pinholes are too small for the DNA to pass through, so that the ion current through the pinholes simply adds in parallel with the primary nanopore current, as illustrated in Figure S6 (Supporting Information).

A TEM image of an 8 nm graphene nanopore, along with a current trace showing DNA translocation through the nanopore device, is given in parts a and b of Figure 2. The electrolyte solution used for these measurements was 1 M KCl, 10 mM Tris, and 1 mM EDTA, pH 9. We added 15 kbp double-stranded DNA (Fermentas NoLimits, Glen Burnie, MD) at a concentration of 1 nM to the analyte reservoir and applied a bias voltage of $V_B = +100$ mV to the other reservoir in order to drive DNA through the pore. The ionic current signal was filtered with a 10 kHz three-pole Bessel filter and then sampled at 50 kHz. We see that the 28 nA open pore current sharply decreases by between ∼500 pA and 1 nA as DNA molecules pass through the graphene nanopore. Translocation events are not observed before the addition of DNA molecules, as demonstrated in Figure S7 (Supporting Information). The overall noise level is much higher for this device than for silicon nitride nanopore devices we have

DOI: 10.1021/nl101046t | *Nano Lett.* **2010,** *10,* 2915–2921

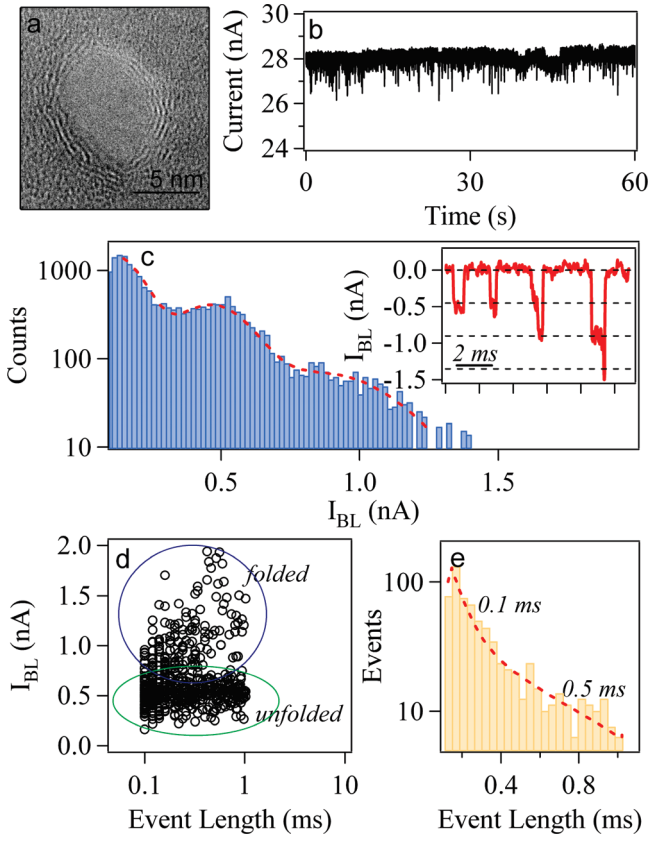

FIGURE 2. DNA translocation through graphene nanopores. (a) TEM image of an ~8 nm graphene nanopore. (b) Time trace of events for nanopore device shown in (a). (c) Histogram of blocked currents for measured translocation events for the same device at $V_B = 100$ mV in 1 M KCl solution. Data are fit using two Gaussian functions with mean values at 0.45 and 0.90 nA. Inset displays concatenated events including some unfolded and folded events which have been observed. I_{BL} values of 0.45, 0.9, and 1.35 nA are indicated with dashed black lines, indicating unfolded, singly folded, and doubly folded entries, respectively. (d) Scatter plot of event length vs event depth for the same device at $V_B = 100$ mV. Regions of unfolded and folded events are highlighted inside the circled areas. (d) Histogram of event lengths for the same device. Data are fit (dashed red line) by a double exponential of the form $a_1 \exp(-t/\tau_1) + a_2 \exp(-t/\tau_2)$ with time constants $\tau_1 = 0.1$ and $\tau_2 = 0.5$ ms. t is the time, and a_1 and a_2 are constants.

measured (see Figure S8 in the Supporting Information), but the DNA capture rate is comparable for both nanopores (~1 event/s for 1 nM and $V_B = 100$ mV). The graphene nanopore noise is dominated by a $1/f$ noise component, which will be discussed later.

A histogram of the measured blocked current signal, I_{BL}, is shown in Figure 2c for the device shown in Figure 2a. Here, I_{BL} is defined as $I_{BL} = \langle I \rangle - \langle I_{open} \rangle$, where $\langle I \rangle$ is the mean pore current during DNA translocation and $\langle I_{open} \rangle$ is the mean pore current 0.1 ms before DNA entry. The data in Figure 2c have been fit with a double Gaussian with mean I_{BL} values of 0.45 and 0.9 nA. These mean values correspond to peaks in the histogram of the current data and indicate two event populations. Examples of both populations are represented in the inset by several representative events. From these events we see that both folded and unfolded events comprise the two populations. The blocked current fraction (i.e., $\langle I_{BL} \rangle / \langle I_{open} \rangle$) is ~5 times smaller than expected based on the relative areas of the DNA molecule (A_{DNA}) and the nanopore[32] (A_p). We calculate an expected value of $A_{DNA}/A_p \sim (2.2\ \text{nm})^2/(8\ \text{nm})^2 = 7.6\%$, compared with a measured blocked current fraction of 1.6%.

Increased baseline open pore current due to pinholes is ultimately responsible for the decreased blocked current fraction. However, the magnitude of the I_{BL} values is 3 times larger than that obtained with similarly sized pores in 40 nm thick SiN membranes at these voltage levels.[33] This increase in I_{BL} is attributed to the thinner graphene membrane, which is ~2 nm thick in Figure 2a. The thinner membrane decreases the overall pore resistance, therefore increasing the magnitude of the current blocked by the translocating DNA molecule. Blocked current values would be even larger for these thin membranes except that the access resistance, the resistance through the electrolyte from the nanopore to the bulk solution, is a significant part of the total resistance of the system (see Figure S6 in Supporting Information). Because of the access resistance, measured I_{BL} values are smaller than expected from the simple approximation that I_{BL} is inversely proportional to membrane thickness.

A scatter plot of event depth as a function of event length for ~600 events measured with the same device is given in Figure 2d. Two clear groupings of events are visible, one centered on $I_{BL} \sim 0.5$ nA (unfolded) and a second centered on ~1 nA (folded). A histogram of the measured event lengths for these events is given in Figure 2e. There is a large variation in the measured event lengths with no clear average value, indicating that the peak value is likely just below the measurement threshold. Two clear populations of events are observed and have been fit with exponential functions[8,32] using time constants of $\tau_1 = 0.1$ ms and $\tau_2 = 0.5$ ms. These time scales correspond to an average DNA velocity of between ~5 and 30 ns/bp, comparable to DNA velocities through other nanopore materials.[34]

We note that while the results in Figure 2 are representative of our measurements of DNA translocation through suspended graphene membranes, the fraction of functional bare graphene nanopores that exhibit detectable DNA translocation is small. Of the 50 bare graphene nanopore devices that we have tested, only ~10% showed DNA translocation. From the remaining pores, 30% had hole defects visible under low-magnification TEM observation, 30% developed tears during the measurement, and 30% did not wet properly, indicated either by a conductance below ~1 nS and/or a highly nonlinear and hysteretic open pore current−voltage measurement. Therefore, despite a large interest in graphene nanopores as electrically addressable ultrathin membrane materials, the low functional yield of pores limits the usability of bare graphene nanopore devices, unless methods of improving membrane stability and wettability are realized.

To address the relatively low yield, we deposited a few nanometer TiO_2 layer on both sides of the graphene membrane

DOI: 10.1021/nl101046t | Nano Lett. 2010, 10, 2915–2921

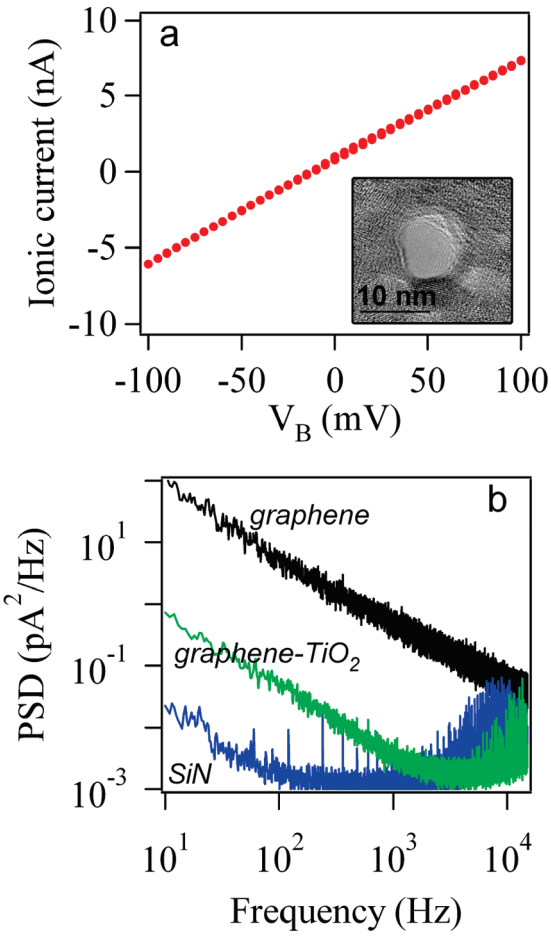

FIGURE 3. Characterization of TiO_2-covered graphene nanopore devices. (a) Current−voltage measurement for a TiO_2-covered graphene nanopore. Inset is a TEM image of this 7.5 nm diameter nanopore. Scale bar is 10 nm. (b) Power spectral density of the pore current for an 8 nm diameter nanopore in a bare graphene device (black) at V_B = 100 mV, a 7.5 nm diameter nanopore in a TiO_2-covered graphene device (green) at V_B = 100 mV, and a 6 nm diameter nanopore in a silicon nitride device (blue) at V_B = 120 mV.

using atomic-layer deposition.[35] ALD has been used a number of times in the context of solid-state nanopores.[15,16,36−40] TiO_2 was chosen because of its excellent wettability with aqueous solutions[41] and superior bonding to graphitic material.[42] ALD has been previously shown to reduce the overall nanopore noise level[36] (particularly the low-frequency, $1/f$ component), presumably by generating a cleaner, more easily wettable surface.[15] An ionic current−voltage measurement of a 10 nm diameter nanopore in graphene coated with 5 nm TiO_2 is shown in Figure 3a, along with a TEM image of the nanopore inset. Following the formation of nanopores, we have observed crystallization of the TiO_2 proximal to the nanopore, as previously observed with nanopores in ALD alumina membranes.[40] The coverage of the graphene membranes with TiO_2 appears conformal based on TEM observation, as shown in Figure S9 (Supporting Information).

Representative power spectral densities (PSD) of open pore current traces are shown in Figure 3b for several devices: a 7.5 nm diameter graphene pore, an 8 nm diameter graphene−TiO_2 pore, and a 6 nm diameter SiN pore. The overall noise level is typically higher for graphene devices than for SiN nanopores tested in the same measurement cell. Particularly, the $1/f$ noise component is especially large for bare graphene devices, extending to the ∼10 kHz frequency range with an exponent of ∼1, as compared with 10−100 Hz for silicon nitride pores. The low-frequency noise power, A, has been calculated for these traces using $S_I/\langle I\rangle^2 = A/f$, where S_I is the current noise up to ∼5 kHz, $\langle I\rangle$ is the mean open pore current, and f is the frequency. We find that $A = 7 \times 10^{-6}$ and 2.5×10^{-7} for bare graphene and TiO_2-covered graphene, respectively, indicating that the covered device has an order of magnitude lower noise power than the bare graphene device. The lower noise power is attributed to the improved hydrophilicity of the TiO_2 surface.[43] Noise power values for the TiO_2-covered device are larger than measured values for SiN nanopores at a similar salt concentration.[44]

Noise due to device capacitance converts the measurement amplifier's voltage noise into current noise, which typically dominates at the higher frequencies. Of all the devices we measured, the graphene-based devices had a higher capacitance than the SiN devices. The capacitance is higher for graphene because the conductive graphene sheet is capacitively coupled to the electrolyte solution. As a result, the entire 5−10 mm^2 graphene area, not just the 0.7 mm^2 area exposed to electrolyte by the measurement cell, forms a capacitor across the SiN and SiO_2 layers to the underlying silicon and electrolyte. Although the 50 × 50 μm^2 SiN membrane is ∼100 times thinner than the rest of the chip, it does not dominate the capacitance because its area is ∼1000 times smaller than a typical graphene sheet.

Example time traces for DNA translocation through three TiO_2-coated graphene nanopore devices are given in Figure 4. TEM images of the nanopores that range in diameter from 5.5 to 8 nm, and concatenated sets of translocation events for each nanopore, are inset. The open pore currents for the devices in Figure 4 do not scale with nanopore diameter, ranging from ∼2.8 nA at 100 mV (Figure 4a) to ∼96 nA at 150 mV (Figure 4c). This is a ∼ 20-fold difference in conductivity. The variation in open pore currents is likely a consequence of the quality difference between graphene membrane starting materials because all other fabrication and preparation steps were consistent. We observe nanoscale differences in graphene grain structure and thickness variation across the relatively large (∼3 μm^2 area, see Figure S3 in Supporting Information) suspended membrane from device to device arising from the nanoscale roughness of the mechanically polished copper foils as evidenced by AFM imaging. This roughness influences the density and rate of formation of pinholes during the TEBAL[26] and/or UV/ozone steps of the device fabrication process.

While some devices without pinholes show open pore currents in the expected range, such as in Figure 4a, others contained pinholes and gave higher open pore currents than

DOI: 10.1021/nl101046t | Nano Lett. 2010, 10, 2915--2921

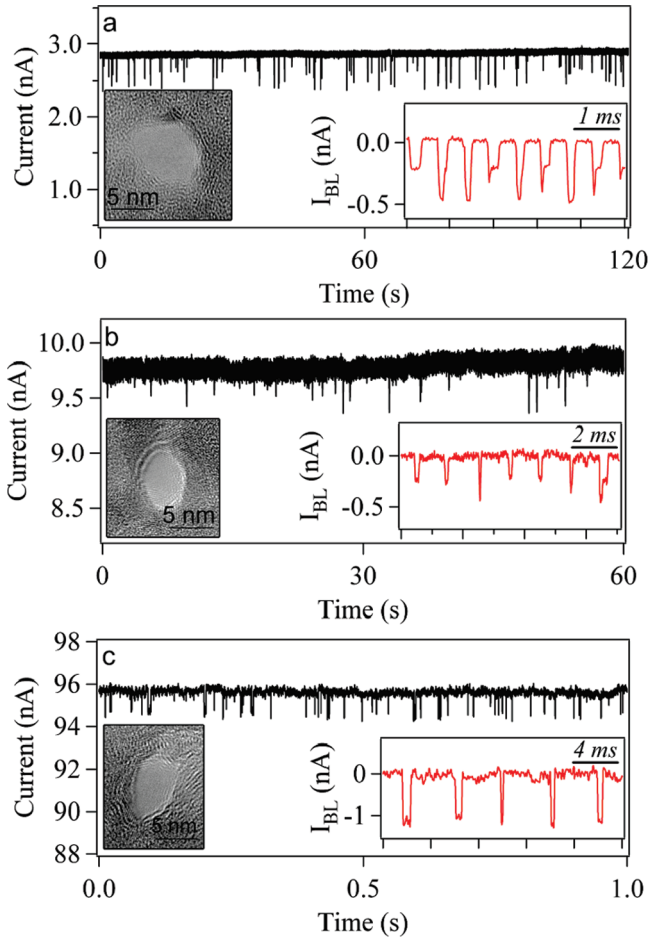

FIGURE 4. DNA translocations through graphene nanopores coated with 5 nm TiO_2. Time traces of ionic current showing DNA translocations for (a) a 7.5 nm nanopore with 1 nM 15 kbp dsDNA, (b) an 8 nm nanopore with 1 nM 15 kbp dsDNA, and (c) a 5 × 7 nm nanopore with 20 nM 400 bp dsDNA. All devices were coated with 5 nm TiO_2. Left inset in each figure is a TEM image of the actual nanopores. Scale bars are 5 nm. Right inset in each figure shows a concatenated sequence of sample events with the open pore current subtracted. V_B for each trace is (a) 100, (b) 100, and (c) 150 mV.

expected. The most striking example of the range of open pore currents that we have measured is the device in Figure 4c. It should be noted that the device in Figure 4c gave the largest measured open pore current of all devices that still gave clear translocation signals. Its inclusion is meant to demonstrate the large range of open pore currents that might be possible in functional devices. For this device we estimate, based on open pore currents and relative nanopore size, that the total pinhole area is 0.08% of the total suspended graphene area. This is a reasonable fraction given that this is the device with the largest open pore current. Rather than a priori excluding such devices, because of their larger-than-expected open pore currents, we have included them here to show that measurable DNA translocation is still possible in devices containing pinholes. This is an important result because it demonstrates the tolerance for device fabrication and graphene quality. Using higher-quality graphene (either CVD or exfoliated) or smaller areas of suspended graphene or eliminating the UV/ozone process in favor of another method may improve the uniformity of open pore currents, if desired.

The data in parts a and b of Figure 4 show translocation of 15 kbp double-stranded DNA (dsDNA) through (a) a 7.5 nm and (b) an 8 nm diameter graphene−TiO_2 nanopore. A similar capture rate was observed when compared with bare graphene and SiN nanopores. I_{BL} values between 200 and 400 pA were observed at $V_B = 100$ mV for these two devices. We have also measured the translocation of much shorter 400 bp dsDNA (Fermentas NoLimits, Glen Burnie, MD), as shown in Figure 4c. Event lengths in Figure 4c are longer than expected, based on the data in parts a and b of Figure 4, due to the decrease in pore area[32] for this device. Here, mean I_{BL} values of over 1 nA are measured for $V_B = 150$ mV. Translocation events for two different DNA lengths, 400 bp and 3000 bp, are additionally shown in Figure S10 (Supporting Information). The amplitude of folded entry (∼1.6 nA) is approximately double the amplitude of unfolded entry (∼0.8 nA), and the appearance of a large fraction of folded and unfolded translocations is in line with previous measurements in solid-state membranes.[45] Despite the differences in baseline current due to varying pinhole density for the pores in Figure 4, the functionality of the devices does not appear to be adversely affected. This is indicated by the similar range of I_{BL} depths for the devices shown in Figure 4, from ∼500 pA to 1.5 nA, even for devices with 2 orders of magnitude difference in open pore current, from ∼3 to 100 nA.

In Figure 5, two-dimensional histograms of event length as a function of I_{BL} are given for 15 kbp dsDNA through a 6 nm graphene nanopore device at V_B = (a) 100 mV and (b) 400 mV. The device was coated with 5 nm of TiO_2, and 1100 and 1800 events were collected and analyzed for (a) and (b), respectively. There are two clear regimes visible in Figure 5a. Unfolded events are clustered at ∼200 pA and folded events are clustered at ∼400 pA, with a mean unfolded event length of ∼200 μs. This corresponds to a translocation speed of 70 bases/μs. The events depicted in Figure 5b are faster and deeper than expected due to the increase in V_B. We measure an average I_{BL} of 1.5 nA at $V_B = 400$ mV and a decreased mean translocation time of ∼100 μs. This is the minimum pulse duration we can measure with the 10 kHz filter in our measurement setup, so the actual translocation time may be shorter.

From the histogram in Figure 5a, there is a clear peak in the blocked current at 200 pA for an applied bias voltage of 100 mV. Though the magnitude of I_{BL} is large, based on this device's open pore current of 10 nA, we calculate that the blocked current accounts for only 2% of the open pore current. This is 1 order of magnitude lower than the expected I_{BL} of 13%, based on a SiN nanopore of the same diameter,[32] further supporting the existence of pinholes in the membrane which increase the baseline open pore current signal. Figure 5c shows the mean I_{BL} as a function

DOI: 10.1021/nl101046t | Nano Lett. 2010, 10, 2915–2921

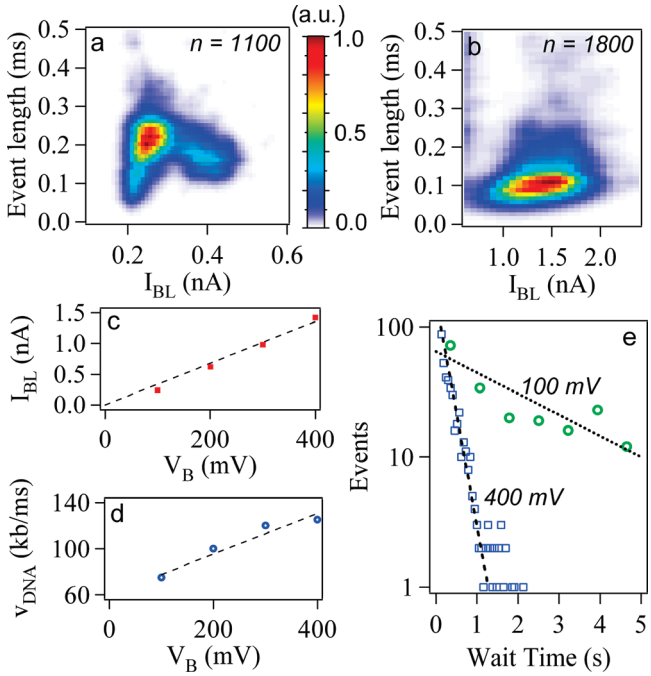

FIGURE 5. Characterization of translocation events for an 8 nm nanopore in a graphene membrane coated with 5 nm of TiO_2. (a) Two-dimensional histogram of event length vs blocked currents for 15 kbp dsDNA at $V_B = 100$ mV. The color scale corresponds to the normalized frequency of events. (b) Two-dimensional histogram of event lengths vs blocked currents at $V_B = 400$ mV. (c) Blocked current, I_{BL}, as a function of V_B. I_{BL} values (red squares) are extracted using a Gaussian fit from current histograms taken at each bias voltage. A linear fit is provided for reference (dashed black line). (d) Translocation velocity, v_{DNA}, as a function of V_B. Velocity values are computed using mean event length values at each bias voltage and DNA length. A linear fit is provided for reference (black dashed line). (e) Histogram of wait times for 250 events at $V_B = 100$ mV (green circles) and 850 events at $V_B = 400$ mV (blue squares). Data were fit with a Poissonian (black dashed line) of the form $\Pi(\lambda,t) = c\lambda \exp(-\lambda t)$, with capture rates $\lambda = 0.3\ s^{-1}$ for $V_B = 100$ mV and $\lambda = 4\ s^{-1}$ for $V_B = 400$ mV, and c is a constant.

of the applied bias voltage for the same device. Mean I_{BL} values are calculated from Gaussian fits to blocked current values, at each bias voltage, as demonstrated in Figure S11 (Supporting Information). The magnitude of the blocked current increases linearly with V_B, as previously observed in SiN pores for DNA in the voltage regime we have tested.[46]

Mean translocation velocity, v_{DNA}, is plotted in Figure 5d as a function of V_B. We observe that the translocation velocity increases linearly with increasing applied bias voltage, as has been observed in SiN nanopores.[47] Mean velocities, v_{DNA}, are calculated by fitting histograms of the measured event lengths at a given V_B and calculating velocity as the length of the molecule (in bases) divided by the most probable event length (in seconds). The event length histograms used to compute v_{DNA} are given in Figure S12 (Supporting Information). A histogram of the wait time between consecutive events is given in Figure 5e for $V_B = 100$ and 400 mV. In both cases the wait time follows a Poissonian distribution, indicative of the uncorrelated nature of the translocations.[8] Wait time decreases with increasing voltage because the distance from the pore at which DNA molecules are captured by the electric field increases with voltage.[36]

In summary, we have presented the first electronic measurements of DNA translocation through graphene nanopores. We found that the current blocked by DNA translocation through graphene nanopores is larger than what has been observed for SiN nanopores of the same diameter, due to the thinness of the graphene membrane. However, bare graphene devices exhibited large ion current noise and suffered from low yield. This could be improved with the use of higher quality graphene material or smaller holes in the supporting SiN membrane to minimize the suspended graphene area. Coating the graphene membrane with a thin TiO_2 layer reduced current noise and provided a more hydrophilic surface, enabling a study of the dynamics of DNA translocation through these pores. Trends of the translocation velocity, current blockage, and capture rate, as a function of applied bias voltage, agree with previous studies carried out with SiN nanopores. Future work will focus on improving the overall reliability of these devices and on utilizing the conductivity of the graphene sheet to create devices for probing DNA molecules. We envision graphene-based nanopore devices that sense and control the electric potential locally at the nanopore and are capable of measuring transverse current across the pore aperture.

Acknowledgment. This work was supported by NIH Grant R21HG004767 and by the JSTO DTRA and the Army Research Office Grant No. W911NF-06-1-0462. This work was also supported in part by the Penn Genome Frontiers Institute, the Nanotechnology Institute of the Commonwealth of Pennsylvania, and a grant with the Pennsylvania Department of Health. The Department of Health specifically disclaims responsibility for any analyses, interpretations, or conclusions. We acknowledge the use of facilities supported by the Nano/Bio Interface Center through the National Science Foundation NSEC DMR08-32802. K.V. acknowledges funding from the NSF-IGERT program (Grant DGE-0221664).

Supporting Information Available. Further details on CVD growth and characterization of graphene, graphene nanopore fabrication and noise characterization, UV/ozone treatment of graphene, ALD of TiO_2, and DNA translocation (including time traces of DNA translocation through both graphene and SiN nanopores, event characterization of short DNA segments in graphene nanopores, and blocked current and event length histograms). This material is available free of charge via the Internet at http://pubs.acs.org.

REFERENCES AND NOTES

(1) Rhee, M.; Burns, M. A. *Trends Biotechnol.* **2006**, *24*, 580.
(2) Healy, K.; Schiedt, B.; Morrison, A. P. *Nanomedicine* **2007**, *2*, 875.
(3) Dekker, C. *Nat. Nanotechnol.* **2007**, *2*, 209.
(4) Branton, D.; Deamer, D. W.; Marziali, A.; Bayley, H.; Benner, S. A.; Butler, T.; Di Ventra, M.; Garaj, S.; Hibbs, A.; Huang, X.; Jovanovich, S. B.; Krstic, P. S.; Lindsay, S.; Ling, X. S.; Mastrangelo, C. H.; Meller, A.; Oliver, J. S.; Pershin, Y. V.; Ramsey, J. M.; Riehn, R.; Soni, G. V.;

DOI: 10.1021/nl101046t | *Nano Lett.* **2010,** *10,* 2915–2921

Tabard-Cossa, V.; Wanunu, M.; Wiggin, M.; Schloss, J. A. *Nat. Biotechnol.* **2008**, *26*, 1146.
(5) Wanunu, M.; Soni, G. V.; Meller, A. In *Springer Handbook of Single-Molecule Biophysics*; Van Oijen, A., Ed.; Springer Publishing: New York, 2009.
(6) Gu, L.-Q.; Shim, J. W. *Analyst* **2010**, *135*, 441.
(7) Siwy, Z. S.; Howorka, S. *Chem. Soc. Rev.* **2010**, *39*, 1115–1132.
(8) Meller, A.; Branton, D. *Electrophoresis* **2002**, *23*, 2583.
(9) Kasianowicz, J. J.; Brandin, E.; Branton, D.; Deamer, D. W. *Proc. Natl. Acad. Sci. U.S.A.* **1996**, *93*, 13770.
(10) Astier, Y.; Braha, O.; Bayley, H. *J. Am. Chem. Soc.* **2006**, *128*, 1705.
(11) Clarke, J.; Wu, H.-C.; Jayasinghe, L.; Patel, A.; Reid, S.; Bayley, H. *Nat. Nanotechnol.* **2009**, *4*, 265.
(12) Zwolak, M.; Di Ventra, M. *Nano Lett.* **2005**, *5*, 421.
(13) Postma, H. W. C. *Nano Lett.* **2010**, *10*, 420.
(14) Chang, S.; Huang, S.; He, J.; Liang, F.; Zhang, P.; Li, S.; Chen, X.; Sankey, O.; Lindsay, S. *Nano Lett.* **2010**, *10*, 1070.
(15) Li, J.; Stein, D.; McMullan, C.; Branton, D.; Aziz, M. J.; Golovchenko, J. A. *Nature* **2001**, *412*, 166.
(16) Venkatesan, B. M.; Shah, A. B.; Zuo, J.-M.; Bashir, R. *Adv. Func. Mater.* **2010**, *20*, 1266.
(17) Storm, A. J.; Chen, J. H.; Ling, X. S.; Zandbergen, H. W.; Dekker, C. *Nat. Mater.* **2003**, *2*, 537.
(18) Novoselov, K. S.; Geim, A. K.; Morozov, S. V.; Jiang, D.; Zhang, Y.; Dubonos, S. V.; Grigorieva, I. V.; Firsov, A. A. *Science* **2004**, *306*, 666.
(19) Han, M. Y.; Özyilmaz, B.; Zhang, Y.; Kim, P. *Phys. Rev. Lett.* **2007**, *98*, 206805.
(20) Cho, S.; Chen, Y.-F.; Fuhrer, M. S. *Appl. Phys. Lett.* **2007**, *91*, 123105.
(21) Meyer, J. C.; Geim, A. K.; Katsnelson, M. I.; Novoselov, K. S.; Booth, T. J.; Roth, S. *Nature* **2007**, *446*, 60.
(22) Fischbein, M. D.; Drndić, M. *Appl. Phys. Lett.* **2008**, *93*, 113107.
(23) Gracheva, M. E.; Melnikov, D. V.; Leburton, J.-P. *ACS Nano* **2008**, *2*, 2349.
(24) Gracheva, M. E.; Vidal, J.; Leburton, J.-P. *Nano Lett.* **2007**, *7*, 1717.
(25) Li, X.; Cai, W.; An, J.; Kim, S.; Nah, J.; Yang, D.; Piner, R.; Velamakanni, A.; Jung, I.; Tutuc, E.; Banerjee, S. K.; Colombo, L.; Ruoff, R. S. *Science* **2009**, *324*, 1312.
(26) Fischbein, M. D.; Drndić, M. *Nano Lett.* **2007**, *7*, 1329.
(27) Wang, S.; Zhang, Y.; Abidi, N.; Cabrales, L. *Langmuir* **2009**, *25*, 11078.
(28) Liu, Z.; Suenaga, K.; Harris, P. J. F.; Iijima, S. *Phys. Rev. Lett.* **2009**, *102*, No. 015501.
(29) Simmons, J. M.; Nichols, B. M.; Baker, S. E.; Marcus, M. S.; Castellini, O. M.; Lee, C.-S.; Hamers, R. J.; Eriksson, M. A. *J. Phys. Chem. B* **2006**, *110*, 7113.
(30) Hashimoto, A.; Suenaga, K.; Gloter, A.; Urita, K.; Iijima, S. *Nature* **2004**, *430*, 870.
(31) Kim, K. S.; Zhao, Y.; Jang, H.; Lee, S. Y.; Kim, J. M.; Kim, K. S.; Ahn, J.-H.; Kim, P.; Choi, J.-Y.; Hong, B. H. *Nature* **2009**, *457*, 706.
(32) Wanunu, M.; Sutin, J.; McNally, B.; Chow, A.; Meller, A. *Biophys. J.* **2008**, *95*, 4716.
(33) Li, J.; Gershow, M.; Stein, D.; Brandin, E.; Golovchenko, J. A. *Nat. Mater.* **2003**, *2*, 611.
(34) Healy, K. *Nanomedicine* **2007**, *2*, 459.
(35) Aarik, J.; Aidla, A.; Uustare, T.; Kukli, K.; Sammelselg, V.; Ritala, M.; Leskelä, M. *Appl. Surf. Sci.* **2002**, *193*, 277.
(36) Chen, P.; Mitsui, T.; Farmer, D. B.; Golovchenko, J.; Gordon, R. G.; Branton, D. *Nano Lett* **2004**, *4*, 1333.
(37) Kim, Y.-R.; Li, C. M.; Wang, Q.; Chen, P. *Front. Biosci.* **2007**, *12*, 2978.
(38) Trepagnier, E. H.; Radenovic, A.; Sivak, D.; Geissler, P.; Liphardt, J. *Nano Lett.* **2007**, *7*, 2824.
(39) Nam, S.-W.; Rooks, M. J.; Kim, K.-B.; Rossnagel, S. M. *Nano Lett.* **2009**, *5*, 2044.
(40) Venkatesan, B. M.; Dorvel, B.; Yemenicioglu, S.; Watkins, N.; Petrov, I.; Bashir, R. *Adv. Mater.* **2009**, *21*, 2771.
(41) Wang, R.; Hashimoto, K.; Fujishima, A.; Chikuni, M.; Kojima, E.; Kitamura, A.; Shimohigoshi, M.; Watanabe, T. *Nature* **1997**, *388*, 431.
(42) Zhang, Y.; Dai, H. *Appl. Phys. Lett.* **2000**, *77*, 3015.
(43) Smeets, R. M. M.; Keyser, U. F.; Wu, M. Y.; Dekker, N. H.; Dekker, C. *Phys. Rev. Lett.* **2006**, *97*, No. 088101.
(44) Smeets, R. M. M.; Keyser, U. F.; Dekker, N. H.; Dekker, C. *Proc. Natl. Acad. Sci. U.S.A.* **2008**, *105*, 417.
(45) Storm, A. J.; Chen, J. H.; Zandbergen, H. W.; Dekker, C. *Phys. Rev. E* **2005**, *71*, No. 051903.
(46) Skinner, G. M.; van den Hout, M.; Broekmans, O.; Dekker, C.; Dekker, N. H. *Nano Lett.* **2009**, *9*, 2953.
(47) Chen, P.; Gu, J.; Brandin, E.; Kim, Y.-R.; Wang, Q.; Branton, D. *Nano Lett.* **2004**, *4*, 2293.

DOI: 10.1021/nl101046t | *Nano Lett.* **2010,** *10,* 2915–2921